Методы повышения качества данных поляриметрических метеорологических радаров

А.В. Рыжков[,2], В.М. Мельников[1,2], Д.С. Зрнич[2]

[1] *Университет Оклахомы, США;*
[2] *Национальная лаборатория по исследованию сильных штормов, США, 120 David L Boren Blvd., Norman, Oklahoma, USA, 73072*

Основные проблемы качества, обсуждаемые в докладе, включают в себя абсолютную калибровку радарной отражаемости Z и дифференциальной отражаемости ZDR, необходимость коррекции на ослабление/дифференциальное ослабление в осадках и устранения ошибок, связанных с частичной блокировкой радарного луча препятствиями. Предлагаются различные методологии для радаров, работающих в S, C, и X диапазонах. Для калибровки Z рекомендуется метод, базирующийся на взаимной зависимости Z, ZDR и удельной дифференциальной фазы KDP в дожде. Обсуждаются пять методик абсолютной калибровки дифференциальной отражаемости. Коррекция на ослабление и блокировку луча осуществляется с использованием KDP и удельного ослабления A, на которые ослабление и блокировка не влияют.

Methods for Improving Data Quality of Polarimetric Weather Radars

Alexander V. Ryzhkov[1,2] , Valery M. Melnikov[1,2], Dusan Zrnic[2]

[1]*University of Oklahoma, USA;*
[2] *National Severe Storms Laboratory, USA 120 David L Boren Blvd., Norman, Oklahoma, USA, 73072*

The issues with data quality addressed in the paper include absolute calibration of radar reflectivity factor Z, absolute calibration of differential reflectivity ZDR, the need for correction for attenuation/differential attenuation in precipitation, and mitigation of partial beam blockage of the radar. Various methodologies are suggested for utilization on weather radars operating at S, C, and X bands. A data-based method for absolute calibration of Z capitalizes on the consistency between Z, ZDR, and specific differential phase KDP in rain. Different techniques for absolute calibration of ZDR are discussed: (1) system internal hardware calibration, (2) "birdbath" calibration with vertically pointing radar, (3) Z – ZDR consistency in light rain, (4) using dry aggregated snow as a natural calibrator for ZDR, and (5) using Bragg scatter as another natural target for calibration. Attenuation and radar beam blockage correction of Z and ZDR is performed using KDP and specific attenuation A which are immune to these factors.

1. Introduction

Dual-polarization Doppler radars become a standard for operational networks of weather radars. Weather applications of dual-polarization radars are summarized by Ryzhkov et al. [1]. First network of polarimetric weather radars operating at S band has been completed in the US in 2013. Since then, similar operational weather radar systems have been either implemented or remain under development in Europe, Asia, and Australia. The Russian Federation follows a trend and, starting from 2011, a full-scale modernization of existing weather radar network by replacing old radars with C-band polarimetric Doppler radars (ДМРЛ-С) is underway (Ефремов и др., [2]; Дядюченко и др., [3]; Жуков и Щукин, [4].

Providing high quality of weather radar data is essential for producing reliable and robust hydrological and meteorological information useful to the scientific and operational communities. The accuracy of quantitative precipitation estimation (QPE) and hydrometeor classification directly depends on the quality of different radar variable estimates. Modern operational Doppler polarimetric radars directly measure radar reflectivity Z, differential reflectivity Z_{DR}, differential phase Φ_{DP}, cross-correlation coefficient ρ_{hv}, Doppler velocity v, Doppler spectrum width σ_v, and linear depolarization ratio *LDR* (in the LDR mode of operation). Specific differential phase K_{DP} is not directly measured but derived from Φ_{DP}. The meaning of listed radar variables is explained in Bringi and Chandrasekar [5], Ryzhkov et al. [1].

The estimates of all these radar variables are obtained in the radar data processor from the time series of successive radar samples within the dwell time interval and are subject to random fluctuations caused by the statistical nature of the radar signal. The uncertainty of such estimates is characterized by bias (or accuracy) and standard deviation (or precision). The latter one is the measure of the "noisiness" of the estimate or the intensity of its temporal and spatial fluctuations. Several factors may cause bias in the estimates of different radar variables. These include (1) radar miscalibration, (2) impact of wet antenna radome, (3) attenuation in atmospheric gases and precipitation, (4) partial beam blockage (PBB), (5) ground clutter contamination, (6) low signal-to-noise ratio (SNR), (7) nonuniform beam filling (NBF), (8) depolarization from propagation in oriented ice crystals, and (9) multipath propagation (three-body scattering). These factors affect differently the biases of various radar variables. In this paper, a brief summary of the measurement errors and the methods to reduce such errors is presented.

2. Absolute calibration of Z

For most important practical applications of polarimetric weather radar, the radar reflectivity factor Z should be calibrated with the accuracy of 1 dB, and differential reflectivity Z_{DR} with the accuracy of 0.2 dB. These generally enable estimating rainfall within 15% accuracy (Ryzhkov et al., [6]). Better accuracy of the Z_{DR} calibration (0.1 dB) might be needed for measurements of light rain or snow.

Polarimetric diversity provides a new method for absolute calibration of Z which was a long-standing problem for single-polarization radars. This methodology rests on the idea that Z, Z_{DR}, and K_{DP} are interdependent in rain and Z can be estimated from K_{DP} and Z_{DR} which are independent of absolute radar calibration. The difference between computed and measured values of Z is considered to be the Z bias. The consistency of Z, Z_{DR}, and K_{DP} in rain can be formulated as a dependence of the ratio K_{DP}/Z on Z_{DR} :

$$\frac{K_{DP}}{Z} = f(Z_{DR}) . \tag{1}$$

In (1), Z and K_{DP} are in linear scale (i.e., $mm^6 m^{-3}$ and deg km^{-1} respectively).

The scatterplots of the ratio K_{DP}/Z versus Z_{DR} simulated from large DSD dataset in Oklahoma for three radar wavelengths and two temperatures, 0°C and 30°C, are illustrated in Fig. 1. It is evident that the dependence in (1) on temperature is negligibly small at S band where the effects of resonance scattering are insignificant. However, the temperature becomes an important factor at C band for $Z_{DR} > 2$ dB and should be taken into account for all Z_{DR} at X band. At S or C bands, Z can be estimated from known K_{DP} and Z_{DR} with the accuracy better than 1 dB if rain does not contain many resonance-size drops.

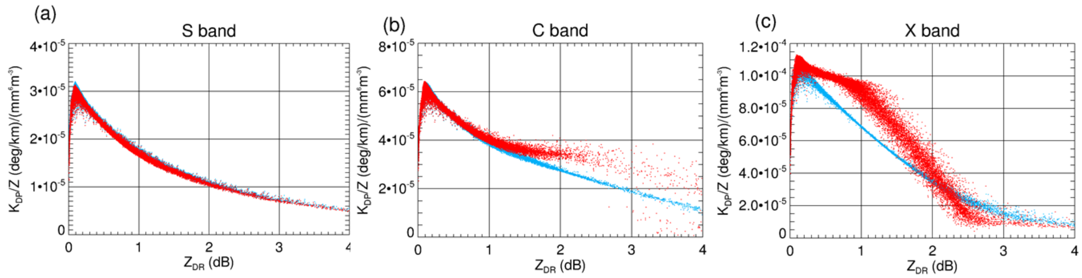

Fig. 1. Scatterplots of K_{DP}/Z versus Z_{DR} at S band (λ = 11.0 cm), C band (λ = 5.45 cm), and X band (λ = 3.2 cm) for raindrop temperature 0°C (blue dots) and 30°C (red dots).

The function $f(Z_{DR})$ can be well approximated by a fourth-order polynomial fit in certain range of Z_{DR} so that (1) can be presented as

$$\frac{K_{DP}}{Z} = 10^{-5}(a_0 + a_1 Z_{DR} + a_2 Z_{DR}^2 + a_3 Z_{DR}^3). \tag{2}$$

In (2), Z_{DR} is in decibels and the coefficients a_0 – a_3 for the S-, C-, and X-band radar wavelengths are listed in Table 1. It is important, that (2) with coefficients from the Table 1 is valid in the Z_{DR} range 0.2 dB to 2 or 3 dB and that different consistency relations should be used for different temperatures at X band.

Because each of the three polarimetric variables in (2) has statistical errors and K_{DP} is notoriously noisy in light rain (especially at longer radar wavelengths) it is instrumental to rewrite (2) as

$$K_{DP} = 10^{0.1Z(dBZ)} f(Z_{DR}) \tag{3}$$

and integrate both sides of (3) over a sufficiently large spatial / temporal domain Ω (Ryzhkov et al., [6]). The integral

$$I_1 = \int K_{DP} d\Omega \tag{4}$$

should be equal to the integral

$$I_2 = \int 10^{0.1Z_m} f(Z_{DR}) d\Omega, \tag{5}$$

if measured reflectivity Z_m is perfectly calibrated. The difference between I_1 and I_2 points to Z bias ΔZ which can be estimated as

$$\Delta Z(dB) = 10\log(I_2 / I_1). \tag{6}$$

if $Z_m = Z + \Delta Z$. Because approximation (2) is valid only in the limited range of Z_{DR} listed in the Table 1, the integrations (4) and (5) should be carried out only over the pixels of data within the appropriate range of Z_{DR} (e.g., between 0.2 and 2.0 dB at C band). It is also required that data in the domain Ω are not biased by low signal-to-noise ratio or contaminated by scatterers other than raindrops. These requirements are satisfied if SNR > 25 dB and ρ_{hv} > 0.99.

Table 1. Coefficients a_0 – a_3 in (2) for S band (λ = 11.0 cm), C band (λ = 5.45 cm), and X band (λ = 3.2 cm).

Frequency band	Temperature (°C)	Z_{DR} range (dB)	a_0	a_1	a_2	a_3
S	0 - 30	0.2 – 3.0	3.19	-2.16	0.795	-0.119
C	0 - 30	0.2 – 2.0	6.70	-4.42	2.16	-0.404
X	0	0.2 – 3.0	11.2	-4.75	0.349	-0.0532
X	10	0.2 – 3.0	10.9	-2.63	-1.22	0.341

X	20	0.2 – 3.0	10.4	0.109	-3.01	0.636
X	30	0.2 – 3.0	9.68	3.07	-4.67	0.869

The methodology of matching the integrals I_1 and I_2 was first tested at S band on a large polarimetric dataset obtained during the Joint Polarization Experiment in Oklahoma and yielded an accuracy of Z calibration within 1 dB (Ryzhkov et al., [6]). To mitigate the impact of attenuation (particularly at C and X bands), Z and Z_{DR} should be either corrected for attenuation using total differential phase Φ_{DP} according to the methods described in Section 4 or only the data radials with sufficiently small span of Φ_{DP} should be used for calibration.

3. Absolute calibration of Z_{DR}

3.1. System internal calibration.

Relative internal calibration of Z_{DR} can be achieved by measuring the differences between gains / losses in the two orthogonal channels. Because the transmission path and reception path differ, separate relative calibration of each is needed. Thus, the power ratio P_{h} /P_{v} downstream of the components that can cause bias in each path needs to be monitored. A change in either ratio would cause a corresponding relative drift in the Z_{DR} bias which is then corrected (Zrnic et al., [7]). An additional step to account for the absolute bias must be made. The procedure is explained next by referring to the diagram in Fig. 2.

The relative values of the power ratios (in dB) are measured at two points. One is at the waveguide couplers $\mathrm{T_{ch}}$ and $\mathrm{T_{cv}}$ on the transmission side; these extract powers from the corresponding H and V waveguides to establish the relative value in the transmission path. The other point is at the output of the two receivers when the signals are injected into the receiving couplers $\mathrm{R_{ch}}$ and $\mathrm{R_{cv}}$ above the low noise amplifiers.

Let the power ratio of outputs at the couplers $\mathrm{T_{ch}}$ and $\mathrm{T_{cv}}$ be

$$\Delta_{\mathrm{T}}(t_0) = 10\log[P\,(\mathrm{Tc_h})/P\,(\mathrm{Tc_v})] \tag{7}$$

where t_0 is a reference time stamp; in its proximity few more initial measurements must be made. $\Delta_{\mathrm{T}}(t_0)$ is measured using one receiver (say H) as in Fig. 2 by switching between the outputs of $\mathrm{T_{ch}}$ and $\mathrm{T_{cv}}$. That way the receiver’s transfer function does not affect the measurement. The $\Delta_{\mathrm{T}}(t_0)$ should be stable over many hours because there are no separate active components in the path up to the couplers.

In the receiver path, a similar procedure is applied (Fig. 2). Note that the signal generator power is split (approximately 50:50) and the exact value at the splitter output is immaterial because the measurement is relative. Thus the power ratio is

$$\Delta_{\mathrm{R}}(t_0) = 10\log[P(\mathrm{Rc_h})/P(\mathrm{Rc_v})], \tag{8}$$

and it is measured immediately after (7) to avoid possible changes between the measurements.

After these two measurements are made, one needs to establish the absolute bias. This is more challenging and few options have been tried. One is from Bragg scatterers (section 3.5) which produce zero Z_{DR}, thus, the overall correct bias is the value of Z_{DR} measured from Bragg scatterers. Let that correct value be $\Delta_{\mathrm{C}}(t_0)$. It needs to be subtracted from the biased estimates denoted with $\hat{Z}_{\mathrm{DR}}$ to obtain the corrected differential reflectivity Z_{DR}:

$$Z_{\mathrm{DR}} = \hat{Z}_{\mathrm{DR}} - \Delta_{\mathrm{C}}(t_0)\,. \tag{9}$$

This correction is valid if (7) and (8) do not change. $\Delta_T(t_0)$ normally does not change and it suffices to check it at intervals of several hours (eight on the WSR-88D). If a change, denoted with $\Delta_{Tb} = \Delta_T(t) - \Delta_T(t_0)$, does occur it should be subtracted, from (9) i.e.,

$$Z_{DR} = \hat{Z}_{DR} - \Delta_C(t_0) - \Delta_T(t) + \Delta_T(t_0)\,. \tag{10}$$

The same reasoning applies to the receiving part of the bias which, however, changes more often, and to catch these relatively fast changes, calibration of the receiving path is made at the end of each volume scan. This, is automated, and produces stable result. Thus, the receiver bias is $\Delta_{Rb}(t_i) = \Delta_R(t_i) - \Delta_R(t_0)$, at the times t_i when volume scans end. The correction requires subtraction of $\Delta_{Rb}(t_i)$ from all the data within the subsequent volume scan, and so on.

The sun can be a reference source and in case the transmitting path is well balanced the Sun flux may be sufficient for absolute calibration. Then the bias Δ_{Sb} revealed from the Sun scan can be substituted for $\Delta_C(t_0)$ in (9).

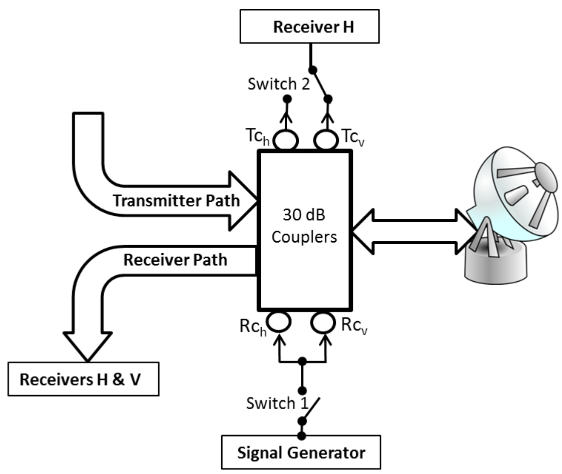

Fig. 2. Transmitter and receiver paths to the antenna. The couplers in the transmitter path Tc_h, Tc_v tap the signals from the H, V waveguides close to the antenna; comparison is made sequentially, via Switch 2, in the H receiver. The signal generator's output is split and injected into the receiver couplers Rc_h, Rc_v located above the low noise amplifiers in the H, V waveguides. During data collection the Switch 1 is open; it closes at the end of volume scans to enable automatic calibration of the receiver path.

3.2. "Birdbath" calibration of Z_{DR}.

Because the mean canting angle of raindrops is close to zero, raindrops appear spherical if viewed at vertical incidence and the measured Z_{DR} in light rain with vertically pointing antenna should be close to 0 dB. Such calibration technique ("birdbath" calibration) is discussed in Gorgucci et al. [8] and Frech et al. [9] among others. This technique may work well only in light rain and in the absence of contamination from ground clutter via antenna sidelobes. Such contamination can cause azimuthal modulation of Z_{DR} for vertically looking rotating antenna. If this is the case, azimuthal averaging is needed for determining the Z_{DR} bias or spectral filtering of the ground clutter components can be applied (Zrnic and Melnikov, [10]).

3.3. $Z - Z_{DR}$ consistency in light rain.

Small raindrops have nearly spherical shape and it is expected that Z_{DR} in light rain dominated by small-size drops is relatively close to zero dB. Therefore, light rain may serve as a natural calibrator for Z_{DR} measurements. This, however, is valid only in a general sense because raindrop size distributions associated with intense size sorting within convective updrafts are skewed towards larger drops and high values of Z_{DR} may be measured in the areas of relatively low Z. Fig. 3 shows Z – Z_{DR} dependencies corresponding to different percentiles of Z_{DR} for a given Z in rain simulated from 47114 DSDs measured in Oklahoma. The simulations are for S band at T = 20°C. The domain between two dashed curves encompasses Z – Z_{DR} pairs of the whole dataset. Thus, Z_{DR} can be as high as 1 dB for Z = 20 dB. Nevertheless, in 80% of cases, Z_{DR} at Z = 20 dBZ stays below 0.4 dB with average value of 0.23 dB.

The Z – Z_{DR} dependencies in rain shown in Figs. 6.3 – 6.5 are valid at S band. Similar analysis at shorter radar wavelengths shows quite similar results for Z < 30 dB (see Table 2).

The procedure for Z_{DR} calibration based on the radar measurements in rain can be easily automated so that the consistency between measured and expected values of Z_{DR} in light rain is checked every radar scan if appropriate data are available. According to the automatic calibration routine implemented on the MeteoFrance operational radar network, the measured median Z_{DR} at Z = 20 - 22 dBZ is compared with its reference value 0.2 dB. It is also possible to estimate the Z_{DR} bias as

$$\Delta Z_{DR} = \frac{1}{6}\sum_{k=1}^{6}[Z_{DR}^{(m)}(k) - <Z_{DR}^{(m)}(k)>] \tag{11}$$

where $<Z_{DR}^{(m)}(k)>$ are median climatological values of Z_{DR} in the kth 2-dB bin of Z shown in Table 2 and $Z_{DR}^{(m)}(k)$ its value estimated from real radar data. Similarly to the self-consistency calibration of Z, the data appropriate for calibration of Z_{DR} should be selected where SNR is sufficiently high (SNR > 20 – 25 dB), differential attenuation is insignificant, and rain scatterers are dominant contributors (i.e., ρ_{hv} > 0.98 – 0.99).

Table 2. Median climatological values of Z_{DR} (dB) for different Z (dBZ) at S, C, and X bands in rain (20 < Z < 30 dBZ).

Z	20	22	24	26	28	30
Z_{DR}(S)	0.23	0.27	0.32	0.38	0.46	0.55
Z_{DR}(C)	0.23	0.27	0.33	0.40	0.48	0.56
Z_{DR}(X)	0.23	0.28	0.33	0.41	0.49	0.58

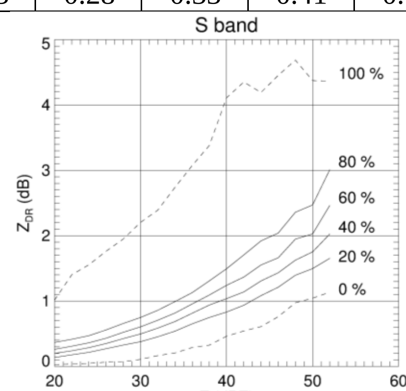

Fig. 3. Z – Z_{DR} dependencies corresponding to various percentiles of Z_{DR} for a given Z in rain. Z and Z_{DR} are simulated at S band from 47144 DSDs measured in Oklahoma.

3.4. Z_{DR} calibration using dry aggregated snow

Dry aggregated snow is known for its small intrinsic Z_{DR} caused by very low density. The study by Ryzhkov et al. [6] indicate that mean Z_{DR} (i.e., averaged over a sufficiently large spatial

/ temporal interval) in aggregated snow usually does not exceed 0.2 dB if Z > 30 dBZ. Dry aggregated snow near the surface does not occur in warm climatic zones. In addition, such a snow should be carefully separated from wet aggregated snow and dry crystallized snow that are characterized by a much higher and more variable Z_{DR}. Nevertheless, dry aggregated snowflakes are commonly present above the melting layer in stratiform clouds (provided that Z > 30 dBZ). Numerous polarimetric radar measurements show that Z_{DR} drops almost to 0 dB 1 – 2 km above the 0°C level where dry aggregated snow is most likely.

Quasi-vertical profiles (QVP, Ryzhkov et al., [11]) of Z_{DR} in aggregates above the melting layer are suitable for monitoring deviation from expected low values. Because QVPs made from azimuthal averages over 360^{o} at high elevations, the accuracy of this measurement is better than 0.1 dB.

3.5. Using Bragg scatter for absolute calibration of Z_{DR}

Melnikov et al. [12] suggest using clear-air radar echoes associated with Bragg scattering for absolute calibration of Z_{DR}. Bragg backscatter from refractive index perturbations at 5 cm scales creates sufficiently strong echo in a convective boundary layer to be detected by 10-cm-wavelength weather radars. These echoes are characterized by intrinsic Z_{DR} equal to 0 dB and cross-correlation coefficient ρ_{hv} very close to 1 making them easily distinguishable from the clear-air echoes caused by biota which have very large Z_{DR} and low ρ_{hv}.

An automated algorithm for estimating Z_{DR} bias from the Bragg scatter was developed and extensively tested on the S-band WSR-88D radars (Richardson et al., [13]). The algorithm yields better accuracy of the Z_{DR} bias estimation than the methods based on the Z_{DR} measurements in light rain and dry snow. Strong Bragg scattering usually occurs at the top of the boundary layer because there the gradients of humidity are largest and mixing by turbulence produces strongest returns. This is seen in Fig. 4 as a distinct layer of enhanced Z and close to zero Z_{DR}. Application of thresholds (Z < 10 dBZ, SNR < 15 dB, ρ_{hv} < 0.98, and $|v|$ > 2 m s^{-1}) and some other criteria identifies data in the layer that are due to the Bragg scatter (Fig. 4b, top left); the histogram of Z_{DR} (Fig. 4, right panel) is indeed centered on 0 dB.

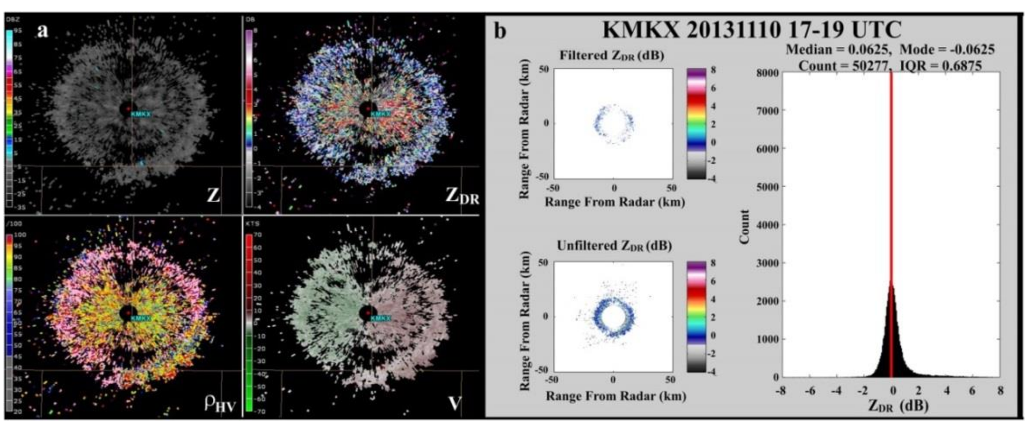

Fig. 4. Example of Bragg scattering observed by the KMKX WSR-88D radar on 10 Nov 2013. (a) The fields of Z (upper left), Z_{DR} (upper right), ρ_{hv} (lower left), and Doppler velocity (lower right) are from conical scans at the 3.5° elevation angle (1852 UTC). Maximum range in the image is ~22 km. (b) The Z_{DR} histogram (right) is from the data (top left corner) which have passed Bragg detection criteria. Data that have passed the SNR > 2 dB threshold are in the bottom left image. (From Richardson et al., [13]).

4. Attenuation correction.

Attenuation of microwave radiation in precipitation may significantly bias the measurements of Z and Z_{DR}, especially at shorter radar wavelengths. Reliable correction of Z and Z_{DR} is required before utilizing these radar variables for quantitative rainfall estimation, hydrometeor classification, microphysical retrievals, etc. Attenuation and differential attenuation in rain cause negative biases in Z and Z_{DR} (ΔZ and ΔZ_{DR} respectively) which can be estimated from the total span of differential phase Φ_{DP} along the propagation path ($\Delta\Phi_{DP}$). Specific attenuation A and specific differential attenuation A_{DP} are generally proportional to specific differential phase K_{DP}:

$$A = \alpha K_{DP} \quad and \quad A_{DP} = \beta K_{DP}\,. \tag{12}$$

Therefore,

$$\Delta Z(r) = 2\int_0^r A(s)ds = 2\alpha\int_0^r K_{\mathrm{DP}}(s)ds = \alpha\Phi_{\mathrm{DP}}(r) \tag{13}$$

and

$$\Delta Z_{\mathrm{DR}}(r) = 2\int_0^r A_{\mathrm{DP}}(s)ds = 2\beta\int_0^r K_{\mathrm{DP}}(s)ds = \beta\Phi_{\mathrm{DP}}(r) \tag{14}$$

if the factors α and β do not change much along the propagation path (0,r) (Bringi et al., [14]).The fact that attenuation biases of Z and Z_{DR} are directly proportional to the differential phase is an advantage of polarimetric radars because it enables accurate quantification of precipitation in the presence of strong attenuation at shorter radar wavelengths (C and X bands).

The factors α and β in (12) are sensitive to the variability of raindrop size distributions and temperature. Typical range of their variability at different radar wavelengths is shown in Table 3. Attenuation correction in the first approximation can be made using "default" or average values in the right column in Table 3. It produces substantial improvement in Z and Z_{DR} compared to the absence of correction. The efficiency of default linear correction using (13) and (14) at C band with $\langle\alpha\rangle = 0.08$ dBdeg^{-1} and $\langle\beta\rangle = 0.02$ dB deg^{-1} is demonstrated in Fig. 5 for the case of a tornadic storm in Oklahoma. The fields of Z and Z_{DR} measured by the C-band OU-PRIME radar show large negative biases before attenuation correction is applied (Fig. 5a,b). The biases are largest along azimuthal directions where total differential phase is highest (Fig. 5c). The corrected fields of Z and Z_{DR} in Fig. 5e,f are consistent with the ones measured by the collocated S-band radar (not shown).

Table 3. Ranges of variability of the factors α and β in rain at S, C, and X bands.

S band	
α = 0.015 – 0.04 dB/deg	<α> = 0.02 dB/deg
β = 0.0025 – 0.009 dB/deg	<β> = 0.004 dB/deg
C band	
α = 0.05 – 0.18 dB/deg	<α> = 0.08 dB/deg
β = 0.008 – 0.1 dB/deg	<β> = 0.02 dB/deg
X band	
α = 0.14 – 0.35 dB/deg	<α> = 0.28 dB/deg
β = 0.03 – 0.06 dB/deg	<β> = 0.05 dB/deg

5. Mitigation of partial beam blockage.

Beam blockage caused by terrain and other obstacles such as buildings and trees limits radar coverage and introduces bias in measurements. Therefore, the quality of the weather radar products such as quantitative precipitation estimate (QPE) is compromised. One of the most common methods for mitigation of partial beam blockage (PBB) uses a digital elevation map (DEM) to estimate the degree of beam blockage at particular azimuths and elevations based on geometry of the beam and its occultation. The DEM-based correction method may not work well if the degree of blockage exceeds 60%. In addition to larger-scale terrain features, small-scale anthropogenic structures (e.g., towers, buildings) and nearby trees that are not accounted for by DEMs can cause additional occultation of the radar beam.

The problem of the partial beam blockage can be resolved more efficiently with the dual-polarization radar than with the single-polarization radar because the former can directly measure differential phase Φ_{DP} and estimate specific attenuation *A* over a propagation path (r_1,r_2) as follows (Ryzhkov et al., [15])

$$A(r) = \frac{[Z_a(r)]^b C(b,PIA)}{I(r_1,r_2) + C(b,PIA) I(r,r_2)} \tag{15}$$

where

$$I(r_1,r_2) = 0.46b \int_{r_1}^{r_2} [Z_a(s)]^b ds\,, \tag{16}$$

$$I(r,r_2) = 0.46b \int_{r}^{r_2} [Z_a(s)]^b ds\,, \tag{17}$$

$$C(b,PIA) = \exp(0.23bPIA) - 1, \tag{18}$$

$$PIA = \alpha [\Phi_{DP}(r_2) - \Phi_{DP}(r_1)] = \alpha\, \Delta\Phi_{DP}\,, \tag{19}$$

where b is a constant and Z_a is the measured radar reflectivity factor which can be biased.

It is evident that the estimate of specific attenuation *A* from a radial profile of Z_a and a total span of differential phase $\Delta\Phi_{DP}$ is totally immune to the *Z* biases caused by attenuation, radar miscalibration, partial beam blockages, and wet radome. Indeed, if attenuated *Z* (Z_a in (15)) expressed in linear scale is multiplied by an arbitrary constant ζ along the propagation path (r_1, r_2), then the value of *A* remains intact because the numerator and denominator in (15) are multiplied by the same factor ζ^b which is cancelled out in the ratio. This property of the *A* estimate by (15) proves to be very beneficial for quantification of rainfall in the partially blocked areas of radar returns if the *A*-based algorithm is used for rainfall estimation. The radar reflectivity factor unbiased by PBB can be estimated from A using the Z(A) relation which is an inverted relation $A = aZ^b$.

The performance of this technique is illustrated in Fig. 6 where the fields of the measured X-band *Z* and Z_{DR} (before correction for attenuation and beam blockage) at antenna elevation 1.5° are displayed along with the fields of Φ_{DP} and radar reflectivity corrected for attenuation and PBB. It is obvious that that the PBB-related *Z* bias in a narrow SE sector is completely eliminated in the panel (c) of Fig. 6.

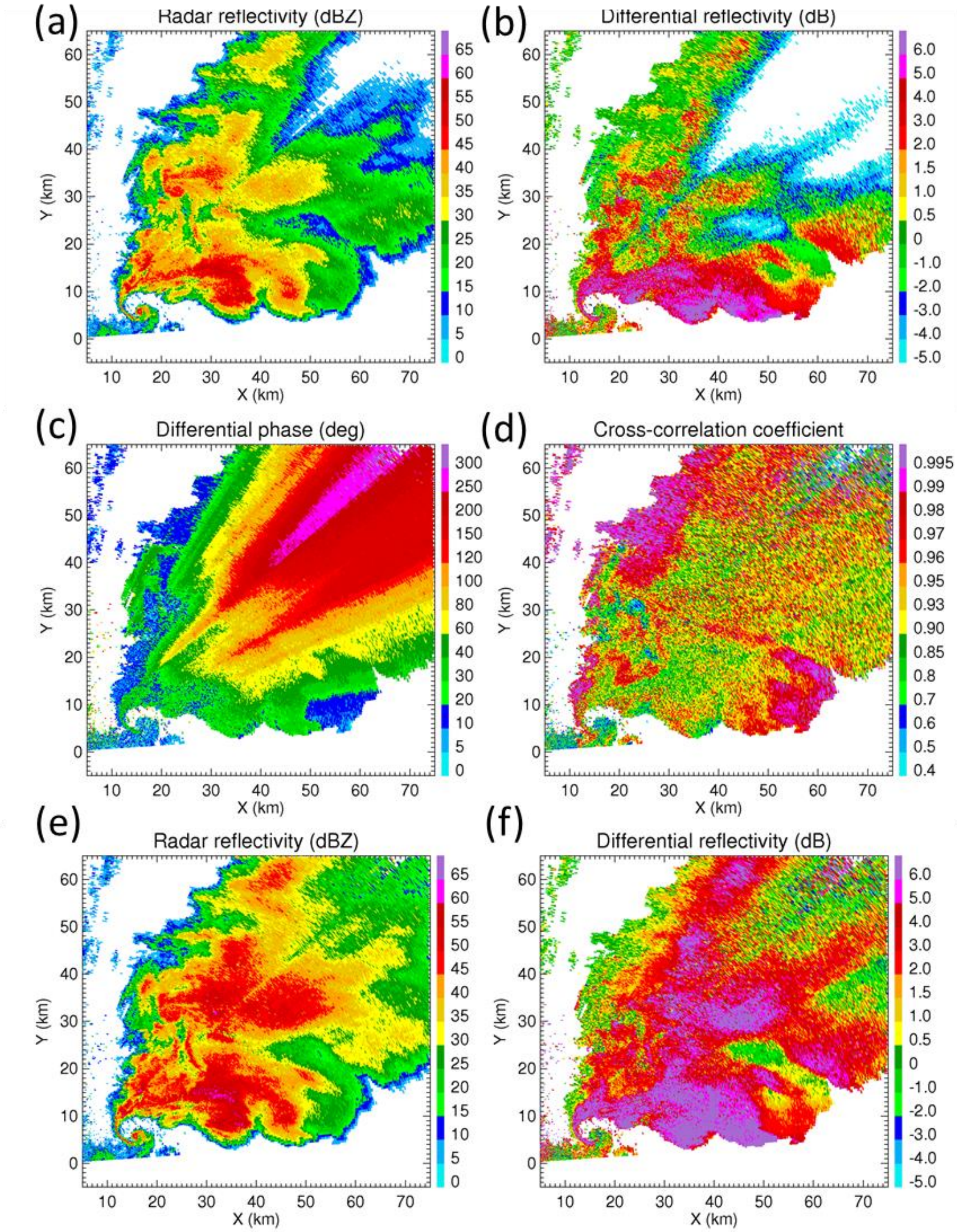

Fig. 5. Composite plot of Z, Z_{DR}, Φ_{DP}, and ρ_{hv} measured by the C-band OU-PRIME radar at elevation 0.5° in the tornadic storm in central Oklahoma on May 10, 2010 at 2042 UTC (panels a – d). The fields of Z and Z_{DR} corrected for attenuation are displayed in panels (e) and (f).

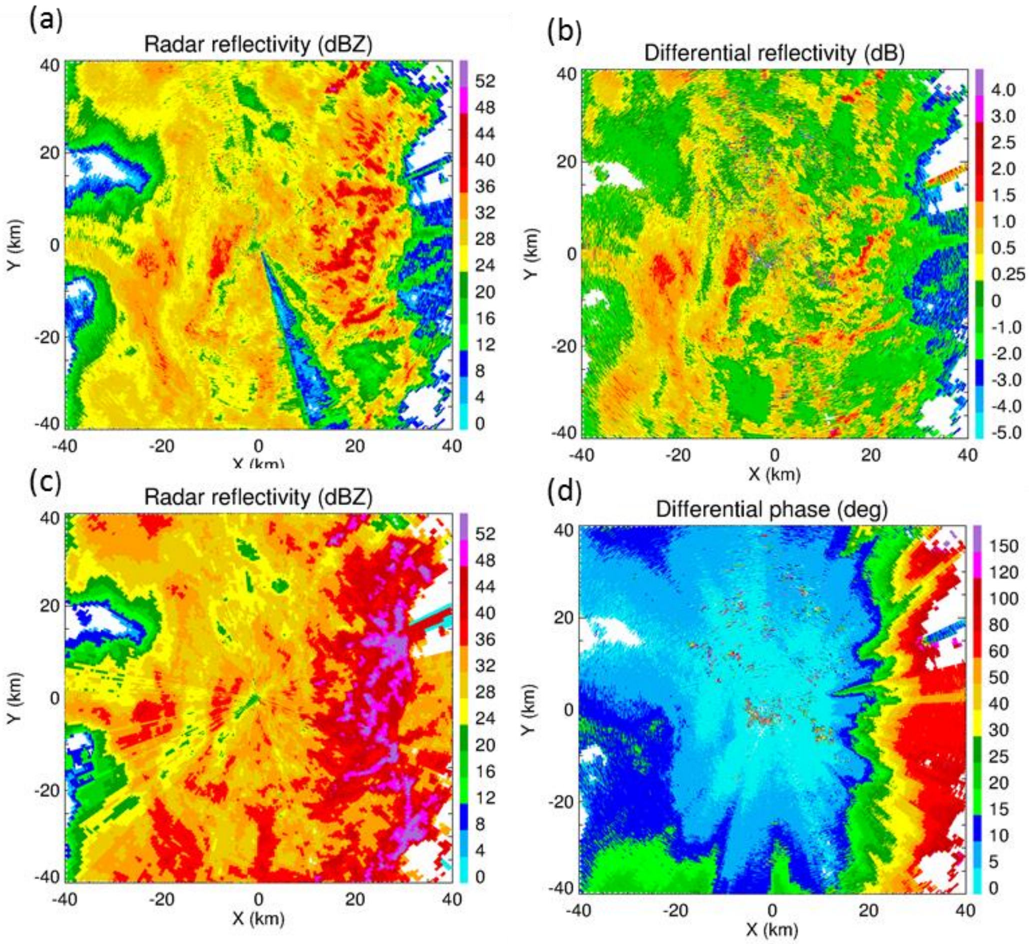

Fig. 6. Composite plot of measured Z and Z_{DR} before correction for attenuation and beam blockage ((a) and (b)), Z after correction (c), and differential phase (d). The measurements are made by the University of Bonn X-band polarimetric radar on June 22, 2011 at 1126 UTC at elevation 1.5°.

6. Statistical errors

Radar signals reflected from weather objects are random. This intrinsic randomness is caused by the motions of individual scatterers in the radar resolution volume. Thermal noise generated by the radar itself and surrounding atmosphere and ground surface also adds to the statistical uncertainty of the estimates of radar variables. To reduce the uncertainty, the estimates of spectral moments and polarimetric variables are calculated from a pulse train of M consecutive samples. These samples are correlated and therefore the reduction in the variance of estimates is smaller than what it would be if there was no correlation between the samples. The variance is inversely proportional to the equivalent number of independent pulses M_I which depends on the wavelength λ, Doppler spectrum width σ_v, and pulse repetition period T. The statistical accuracy of the polarimetric radar variables also depends on the correlation between the horizontally and vertically polarized components of the signal which is quantified by the cross-correlation coefficient ρ_{hv}.

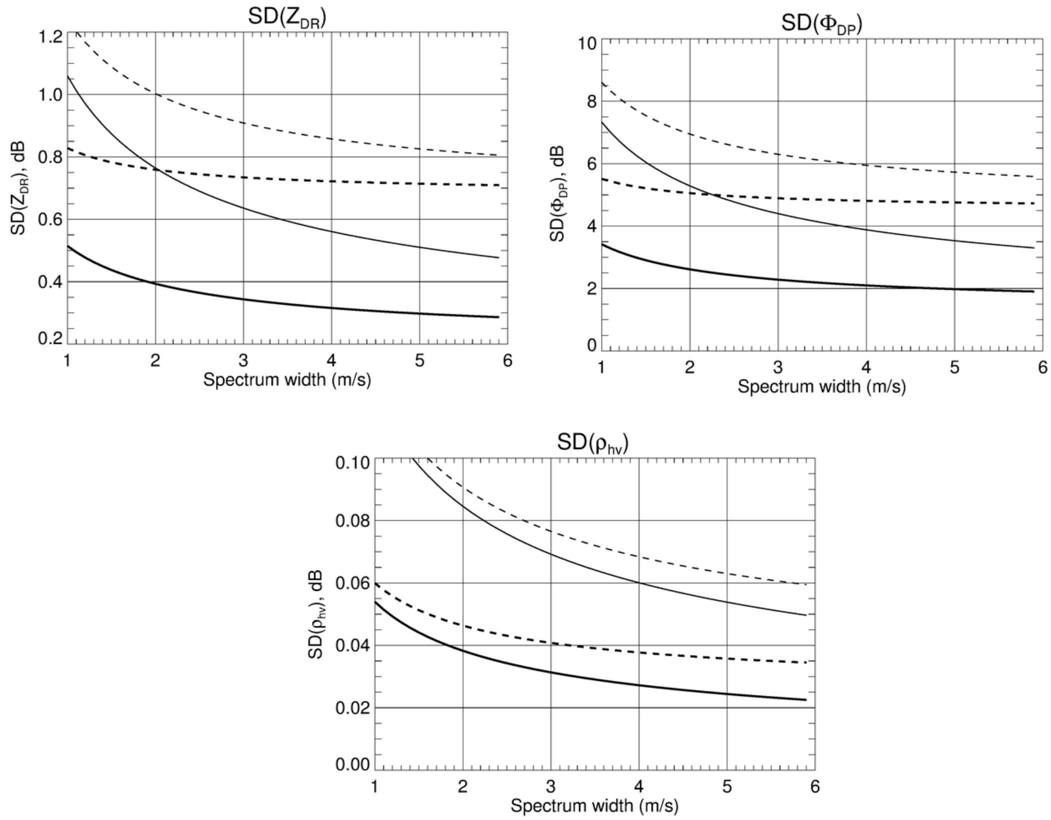

Fig. 7. Standard deviations of the estimates of Z_{DR}, Φ_{DP}, and ρ_{hv} as functions of Doppler spectrum width for different values of ρ_{hv} and SNR at S band (λ = 11 cm) for PRF = 321 Hz and M = 17. Solid lines – SNR = 20 dB, dashed lines – SNR = 10 dB; thick lines – ρ_{hv} = 0.99, thin lines – ρ_{hv} = 0.95.

Relatively simple and compact formulas for the standard deviations of the estimates of radar reflectivity Z, mean Doppler velocity v, spectrum width σ_v, differential reflectivity Z_{DR}, differential phase Φ_{DP}, and cross-correlation coefficient ρ_{hv} can be obtained for high values of signal-to-noise ratio (SNR > 20 dB) if the radar simultaneously transmits and receives H and V waves:

$$SD(Z) = \frac{3.24}{(\sigma_{vn} M)^{1/2}} \quad (\mathrm{dB}), \tag{20}$$

$$SD(v) = 0.20\left(\frac{\lambda \sigma_{v}}{MT}\right)^{1/2} \quad (\mathrm{m\ s^{-1}}), \tag{21}$$

$$SD(\sigma_{v}) = 0.16\left(\frac{\lambda \sigma_{v}}{MT}\right)^{1/2} \quad (\mathrm{m\ s^{-1}}), \tag{22}$$

$$SD(Z_{DR}) = 4.62\left(\frac{1-\rho_{hv}^{2}}{\sigma_{vn} M}\right)^{1/2} \quad (\mathrm{dB}), \tag{23}$$

$$SD(\Phi_{DP}) = 30.3\left(\frac{\rho_{hv}^{-2}-1}{\sigma_{vn} M}\right)^{1/2} \quad (\mathrm{deg}), \tag{24}$$

$$SD(\rho_{hv}) = 0.53 \frac{1-\rho_{hv}^2}{(\sigma_{vn} M)^{1/2}}, \tag{25}$$

where $\sigma_{vn} = 4\sigma_v T / \lambda$ is the normalized spectrum width, λ is the wavelength (in m), T is the pulse repetition period (in sec), and M is the number of pulses. The dependencies of the standard deviations of the estimates of Z_{DR}, Φ_{DP}, and ρ_{hv} on the Doppler spectrum width for different values of ρ_{hv} and SNR at S band are in Fig. 7. The calculations have been made for a typical surveillance scan of the S-band WSR-88D radar with pulse repetition frequency PRF = 321 Hz and M = 17. The standard deviations of all three variables are quite high for such a short dwell time, therefore additional spatial averaging (typically along a radial) is needed to obtain robust estimates of Z_{DR}, Φ_{DP}, and ρ_{hv}.

References

1. Ryzhkov A., Schuur T., Melnikov V., Zhang P., Kumjian M. Weather applications of dual-polarization radars / Радиотехнические и телекоммуникационные системы, 2016, №2. –С. 28-33.

2. Ефремов В.С., Вовшин Б.М., Вылегжанин И.С., Лаврукевич В.В., Седлецкий Р.М. Поляризационный доплеровский метеорологический радиолокатор С-диапазона со сжатием импульсов / Журнал радиоэлектроники, № 10, 2009. -4 с.

3. Дядюченко В.Н., Вылегжанин И.С., Павлюков Ю.Б. Доплеровские радиолокаторы в России / Наука в России. 2014. № 1. –С.23-27.

4. Жуков В.Ю., Щукин Г.Г. Состояние и перспективы сети доплеровских метеорологических радиолокаторов / Метеорология и гидрология, N 2, 2014. С.92 – 100.

5. Bringi, V. and V. Chandrasekar, 2001: Polarimetric Doppler Weather Radar: Principles and Applications. Cambridge University Press, 636 pp.

6. Ryzhkov, A.V., S.E. Giangrande, V. M. Melnikov, and T.J. Schuur, 2005: Calibration issues of dual-polarization radar measurements. *J. Atmos. Oceanic Technol.,* 22, 1138 – 1155.

7. Zrnic, D., V. Melnikov, and J. Carter, 2006: Calibrating differential reflectivity on the WSR-88D. *J. Atmos. Oceanic Technol.,* 23, 944 – 951.

8. Gorgucci, E., G. Scarchilli, and V. Chandrasekar, 1999: A procedure to calibrate multiparameter weather radar using properties of the rain medium, *IEEE Trans. Geosci. Remote Sensing*, 37, 269 – 276.

9. Frech, M., M. Hagen, and T. Mammen, 2017: Monitoring the absolute calibration of a polarimetric weather radar. *J. Atmos. Oceanic Technol*., 34, 599 – 615.

10. Zrnic, D.S., and V.M. Melnikov, 2007: Ground clutter recognition using polarimetric spectral parameters. 33rd Conference on Radar Meteorology, AMS, Cairns, Australia, 2007.

11. Ryzhkov, A., P. Zhang, H. Reeves, M. Kumjian, T. Tschallener, C. Simmer, S. Troemel, 2016: Quasi-vertical profiles – a new way to look at polarimetric radar data. *J. Atmos. Oceanic Technol.,* 33, 551 – 562.

12. Melnikov, V., R. Doviak, D. Zrnic, and D. Stensrud, 2011: Mapping Bragg scatter with a polarimetric WSR-88D. *J. Atmos. Oceanic Technol*., 28, 1273 – 1285.

13. Richardson, L., J. Cunningham, W. Zittel, R. Lee, R. Ice, V. Melnikov, N. Hoban, and J. Gebauer, 2017: Bragg scatter detection by the WSR-88D. Part I: Algorithm development. *J. Atmos. Oceanic Technol.,* 34, 465 – 478.

14. Bringi, V.N., V. Chandrasekar, N. Balakrishnan, and D. S. Zrnic, 1990: An examination of propagation effects in rainfall on polarimetric variables at microwave frequencies. *J. Atmos. Oceanic Technol*., 7, 829-840.

15. Ryzhkov, A., M. Diederich, P. Zhang, and C. Simmer, 2014: Utilization of specific attenuation for rainfall estimation, mitigation of partial beam blockage, and radar networking. *J. Atmos. Oceanic Technol.*, 31, 599 – 619.